

Dual frequency 230/690 GHz interferometry at the Submillimeter Array

Todd R. Hunter, John W. Barrett, Raymond Blundell, Robert D. Christensen, Robert S. Kimberk, Steve Leiker, Daniel P. Marrone, Scott N. Paine, D. Cosmo Papa, Nimesh Patel, Patricia Riddle, Michael J. Smith, T.K. Sridharan, C.-Y. Edward Tong, Ken H. Young and Jun-Hui Zhao
 Harvard-Smithsonian Center for Astrophysics
 60 Garden Street
 Cambridge, MA 02138 USA
 Email: thunter@cfa.harvard.edu

Abstract—The Submillimeter Array (SMA), a collaboration between the Smithsonian Astrophysical Observatory and the Academia Sinica Institute for Astronomy and Astrophysics of Taiwan, is an eight-element radio-interferometer designed to operate throughout the major atmospheric windows from about 180 to 900 GHz. In an effort to mitigate the effects of atmospheric instabilities which limit the phase coherence of the array especially in the higher frequency bands, the array was designed to allow simultaneous operation of a low frequency receiver (< 350 GHz) with a high frequency receiver (> 330 GHz). The overlap region of 330-350 GHz was included to facilitate dual polarization measurements in the frequency range considered to offer the highest sensitivity for continuum observations with the array.

So far, the array is equipped with working SIS receivers covering the frequency ranges 176-250 GHz, 260-355 GHz, and 600-700 GHz, and single frequency operation has been routine in the lower two frequency bands for the past year. More recently, with the completion of IF hardware required to make full use of the SMA cross-correlator, dual receiver operation became possible. We have since made a number of Galactic and extragalactic astronomical observations in dual-band mode with the hopes of using the 230 GHz receiver as a phase reference to enable improved interferometry in the 650 GHz band. We will present the current antenna and receiver performance, some of the first interferometric images in the 650 GHz receiver band, and our initial attempts at phase referencing.

I. INTRODUCTION

The Submillimeter Array (SMA), a collaboration between the Smithsonian Astrophysical Observatory and the Academia Sinica Institute for Astronomy and Astrophysics, is an eight-element, heterodyne radio-interferometer designed to operate throughout the major atmospheric windows from about 180 to 900 GHz. It is the first and only imaging interferometer to operate in the submillimeter band. The general design and operation of the SMA has been described previously [1]. Located near the 4200-meter summit of Mauna Kea, Hawaii, the array was dedicated in November 2003 and initial science results were collected in a 2004 special issue of *The Astrophysical Journal* [2]. The first SMA results at 690 GHz were published in 2004 based on observations of the carbon star IRC+10216 obtained with only three antennas [3]. Since that time, the second IF path of the SMA has been built and commissioned and improvements to the 690 GHz receivers

TABLE I
 ANTENNA PERFORMANCE AS MEASURED BY HOLOGRAPHIC SURFACE RMS (LEFT COLUMN), AND BY APERTURE EFFICIENCY SCANS ON CELESTIAL OBJECTS (RIGHT COLUMNS).

Antenna Number	RMS surface (μm)	Aperture efficiency (%)	
		230 (GHz)	345 GHz
1	15	77	68
2	14	74	67
3	15	75	61
4	18	73	64
5	20	75	60
6	22	74	60

and local oscillator (LO) control hardware have enabled fully-remote, dual-frequency operation for the first time. With this capability, the prospects for “phase referenced calibration” (i.e. scaling the measured atmospheric phase from a low frequency band to a high frequency band) can now be evaluated. This paper summarizes the present system and presents the first results obtained during a special observing campaign during January-February 2005.

II. SYSTEM DETAILS

A. Antenna performance

The SMA 6-meter antennas are composed of 72 machined aluminum reflector panels with 4 adjusting screws per panel. The surface is accurately measured (to 8 μm RMS) via near-field holography and the required screw adjustments to correct the surface are computed [4]. In preparation for 650 GHz work, all antennas were adjusted in this manner to improve the surface accuracy. As of February 2005, all antennas were better than 22 μm RMS with the best antenna being 14 μm RMS (see Table I). Confirmation of the antenna surface accuracy, especially at elevations different from the beacon (i.e. > 20 deg), has been obtained via aperture efficiency measurements on celestial objects (planets).

B. Optical alignment

In order to use two receivers simultaneously, the mixer feedhorns must be aligned on the sky to within a fraction of the primary beamsizes of the low frequency receiver (55''

TABLE II
FEED OFFSET TERMS MEASURED ON THE SMA ANTENNAS.

Antenna Number	345 Rx vs 230 Rx		690 Rx vs 230 Rx	
	A_1 (")	A_2 (")	A_1 (")	A_2 (")
1	-0.2	+6.1	-2.7	+7.0
2	+4.3	+2.1	-0.85	+1.6
3	-0.7	-1.1	+4.1	-0.8
4	-5.3	+4.9	-2.2	+3.6
5	-3.9	-1.3	+4.8	-3.4
6	-0.1	+4.6	+4.4	+3.4

at 230 GHz, or $36''$ and 345 GHz). Alignment of the receiver feeds is done using near-field vector beam measurements in the laboratory [5]. This method produces beams aligned to within $5''$ on the sky, as demonstrated by pointing calibration performed in single-dish mode on each SMA antenna. Table II lists the feed offset terms measured on each of the six SMA antennas used during the recent 650 GHz campaign. The feed offsets are modelled by two parameters: the radial misalignment r in arcseconds, and the phase angle ϕ of this misalignment in degrees. These parameters are combined into two terms: $A_1 = r \cos(\phi)$ and $A_2 = r \sin(\phi)$, which translate into azimuth and elevation offsets: $\text{azoff} = A_1 \sin(\text{Elev}) + A_2 \cos(\text{Elev})$, $\text{eloff} = A_1 \cos(\text{Elev}) - A_2 \sin(\text{Elev})$. The repeatability of the feed offset measurements is $1 - 2''$. During dual-frequency observations, the antennas are pointed such that the high frequency receiver is aimed at the target. The largest resulting pointing error for the 230 GHz feed ($7''$) corresponds to less than 5% loss due to primary beam attenuation. At 345 GHz, the largest pointing error ($6''$) corresponds to less than 8% loss.

C. Mixer performance

In all three bands, the SMA receivers contain double-sideband mixers fabricated with niobium SIS junctions (cooled to 4.2 K) followed by low-noise HEMT amplifiers. The pumped I/V characteristics of these junctions in the field are shown in Figure 1. The IF of our receivers is 4-6 GHz, and the downconverter electronics and correlator can process the full 2 GHz of bandwidth in each sideband. The mixer performance in the IF passband was measured in each of the antennas via the Y-factor method. The passband response was recorded on a spectrum analyzer, first toward an ambient temperature load, and second toward a liquid nitrogen temperature load. A representative plot is shown in Figure 2. The typical receiver temperature (averaged across the IF band) was 300-400 K, or about ten times the quantum limit. In good dry weather conditions on Mauna Kea ($\tau_{225\text{GHz}} < 0.05$), this level of performance results in system temperatures as low as 900-1200 K near zenith. As an example, Figure 3 shows a plot of the 684 GHz system temperatures and the 225 GHz zenith opacity vs. time during the nighttime observations of February 16, 2005.

D. Motorized LOs

The automation of the low-frequency (230 and 345 GHz) LO chains has been described previously [6]. The 690 GHz LO

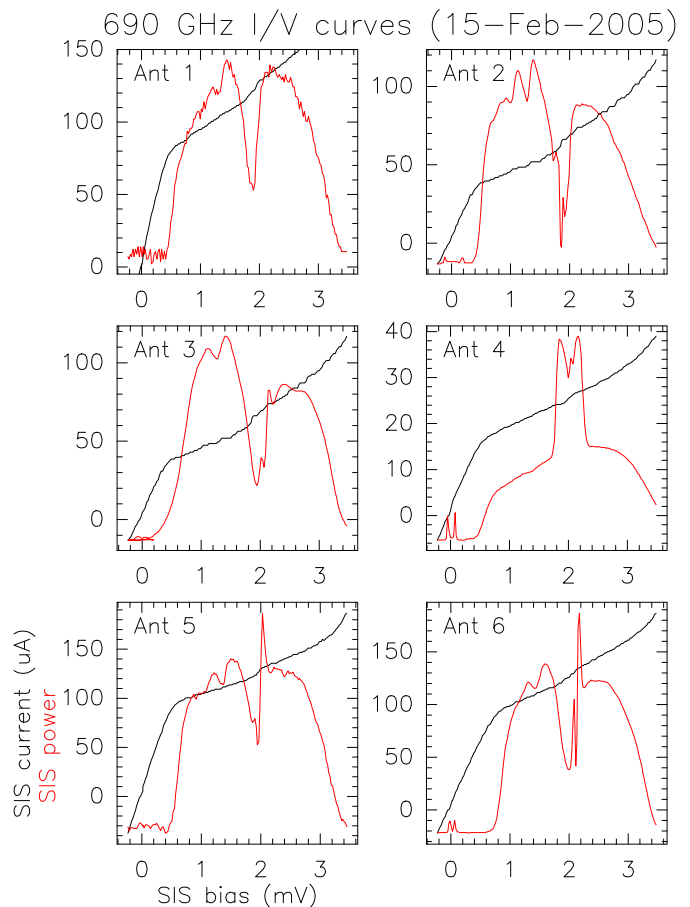


Fig. 1. SIS mixer current vs. bias voltage (black line) and SIS mixer power vs. bias voltage (red line) characteristics of the 650 GHz receivers on the SMA as measured remotely in the field. The SIS power is plotted in arbitrary units.

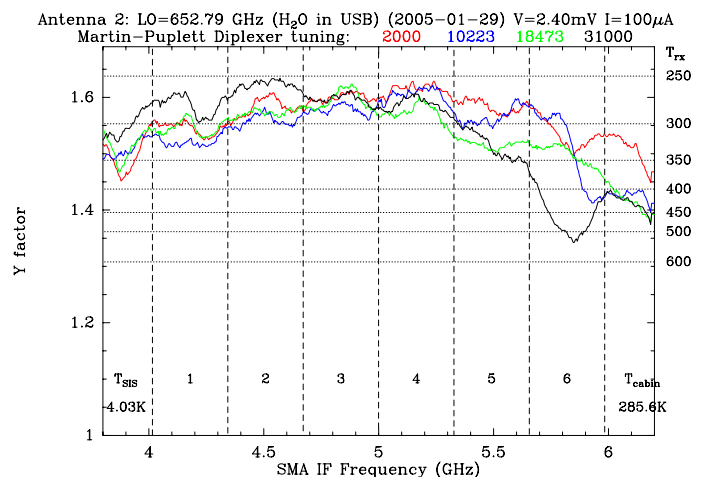


Fig. 2. Receiver temperature as a function of the IF passband (x-axis) and the Martin-Puplett diplexer tuning positions (colored lines) as measured with an HP8563 spectrum analyzer in the field in one of the SMA antennas. The data were obtained using the traditional y-factor method by taking the ratio of two traces: one observing an ambient temperature load and one observing a liquid nitrogen temperature load.

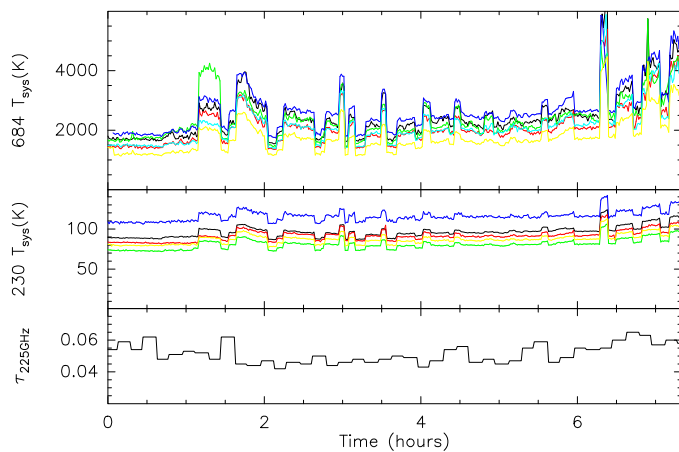


Fig. 3. System temperatures on each of the six antennas at 684 GHz (top panel) and 230 GHz (middle panel) during the night of February 16, 2005. The maximum elevation of the target source (Sgr A*) was only 42 degrees above the horizon (i.e. 1.5 airmasses). For reference, the zenith opacity at 225 GHz as measured by the tipping radiometer at the Caltech Submillimeter Observatory is also plotted (lower panel).

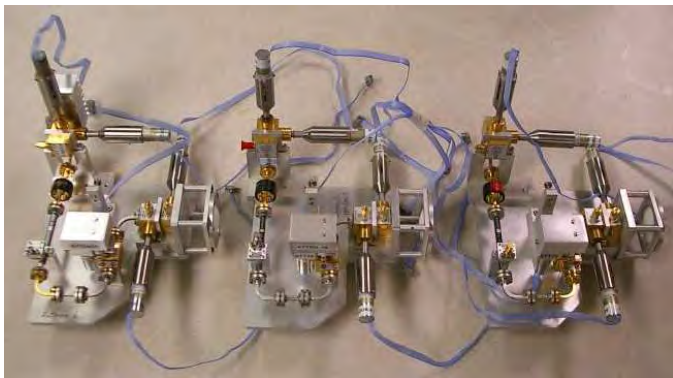


Fig. 4. Three of the six motorized 600-700 GHz LO chains installed on the SMA. At the top is the Gunn oscillator with two linear actuators at right angles to one another. Next is a waveguide isolator followed by a coupler to the PLL harmonic mixer. The vane attenuator is driven by a rotary motor via a gear assembly. The following doubler and tripler stages each have one linear actuator. The LO radiation exits through the lens at the right. Not shown is the Martin-Puplett diplexer which combines the LO and the signal ahead of the cryostat vacuum window.

chains have now been automated in a similar fashion. Each LO chain consists of six motorized components including a Gunn oscillator (2 motors), a vane attenuator (1 motor), a doubler (1 motor), a tripler (1 motor) and Martin-Puplett diplexer (1 motor). A photo three of the LO chains is shown in Figure 4.

E. Dual IF operation

One of the major challenges facing millimeter and sub-millimeter interferometers is fluctuations in atmospheric path length caused by water vapor [7]. Such path length changes result in phase changes which ultimately limit the angular resolution and sensitivity of the instrument. The standard technique of phase referencing at the observed frequency can remove slow drifts in atmospheric and instrumental phase (on

timescales of minutes). However, as one observes at higher frequencies, the phase drifts increase in magnitude, the typical system sensitivities degrade, and the number of calibrators becomes sparse. All of these factors tend to limit the effectiveness of the standard phase referencing technique. The SMA telescope offers the benefit of two independent IF paths (via fiber optics) from the antennas to the correlator which allows simultaneous observations at two widely separated frequencies, or (eventually) dual-polarization observations in the 330-350 GHz range. Observations at different frequencies enable the possibility of simultaneous phase referencing from low frequency where the system sensitivity and stability are the best to high frequency where the tropospheric phase fluctuations are the largest. Recently, this concept has been applied successfully in astronomical very long baseline interferometry (VLBI) experiments by using non-simultaneous, but rapidly time-interleaved observations at 15, 43 and 86 GHz [8]. This interleaving concept has also been considered for use in the Atacama Large Millimeter Array (ALMA) in the future [9]. However, the major drawback of interleaved observations is the frequent receiver retuning which requires some finite amount of time during which the instrumental and atmospheric phases may change significantly. By design, the unique capability of the SMA of **simultaneous** observations at two frequencies offers the best chance at proving the utility of phase referencing in the submillimeter regime.

III. OBSERVATIONS AND RESULTS

A. Conditions and targets

A block of SMA time from January 25 to February 20, 2005 was dedicated to dual-frequency commissioning and observations. The first dual-frequency fringes with five antennas (ten baselines) were recorded on January 28 on the astronomical maser source W Hydra. The SiO $J=5-4$, $v = 1$ maser was observed at 215.596 GHz, and the H₂O $v_2 = 1, 1_{1,0} - 1_{0,1}$ maser was observed at 658.007 GHz. After this initial success, the sixth antenna became operational and the weather conditions became favorable for extensive observations of other astronomical targets from February 14 to 20. The array was configured in the “compact” formation which provides a synthesized beamwidth of 1.1 by 1.2 arcsecond (for sources of moderate northerly declination). Unprojected baseline lengths ranged from 16 to 69 meters. Observations in the CO $J=6-5$ transition were acquired of the nearby Classical T Tauri star TW Hydra, the protoplanetary nebula CRL618, the high-mass star-forming region Orion KL, the low-mass star-forming region IRAS 16293-2422 and the ultraluminous infrared galaxy Arp 220. The Galactic Center source Sgr A* was observed in the continuum at 684 GHz. Finally, the massive star-forming region G240.31+0.07 and the evolved star VY Canis Majoris were observed in the C¹⁸O $J=6-5$ transition. In each case, the typical on-source integration times were three hours. Detailed results from these observations will be presented elsewhere. As an example of the data quality, an image of the Galactic Center point source Sgr A* is shown in Figure 5. This image was produced via standard phase referencing at 684 GHz between

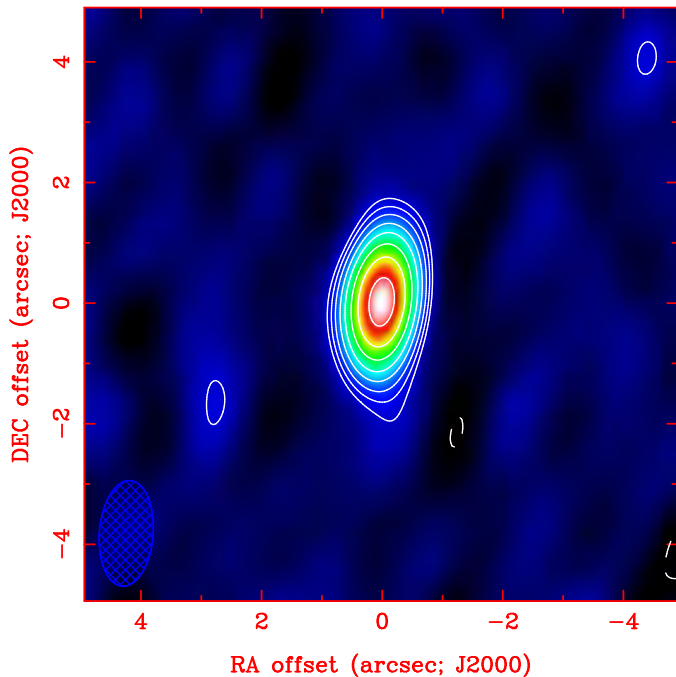


Fig. 5. Contour plot of the Galactic Center radio source Sgr A* observed in 684 GHz continuum emission. Levels are -5, -3.5, 3.5, 5, 7, 10, 14, 20, 28, and 40 σ , with $\sigma = 0.06$ Jy and peak flux density of 2.7 Jy. One Jy is $10^{-26} \text{Wm}^{-2} \text{Hz}^{-1}$. Total integration time is about 3 hours. The synthesized beamwidth of the interferometer is shown in the lower left corner. The offsets are relative to the J2000 source position of 17:45:40.0409, $-29:00:28.118$.

the target and strong calibrators (in this case, Ganymede and Ceres, which were 68° and 41° distant, respectively), followed by phase-only self-calibration on the target itself.

B. Comparison of 230/690 GHz phase

Ultimately we are interested in whether the phase variations at $\nu_1 = 230$ GHz due to fluctuations in the water vapor column above the antennas can be used to calibrate the proportionally larger phase variations that these fluctuations cause at $\nu_2 = 690$ GHz. To first order, the expected scaling of the phase variations equals the ratio of the frequencies (i.e., the non-dispersive case). This is because the effect of introducing a small amount of water vapor above one antenna is to add a (nearly) frequency independent amount of excess propagation path L , which corresponds to a phase delay of L/λ radians where $\lambda = c/\nu$. So the ratio of phases in the two bands is $(L_1/\lambda_1)/(L_2/\lambda_2)$. If $L_1 \approx L_2$, then the ratio becomes $\lambda_2/\lambda_1 = \nu_1/\nu_2$. In fact, the actual value of L is a function of frequency, although it only varies significantly near strong atmospheric water lines [10], [11]. However, because the 650 GHz window sits between two major water lines, the variations are significant and one should not cancel L_1/L_2 in the above formula. So the actual phase ratio we expect is $(L_1/L_2) * (\lambda_2/\lambda_1)$. Figure 6 shows the theoretical ratio L_1/L_2 computed for observations in the 650 GHz band from the

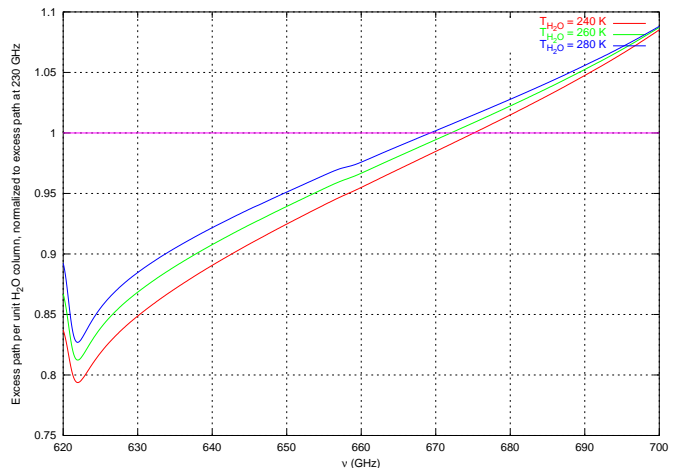


Fig. 6. Calculation of the theoretical excess path per unit water vapor column in the 620-700 GHz observing window, normalized to the excess path at 230 GHz. The three curves correspond to different water vapor temperatures in the model. The largest deviation from unity ratio occurs near water vapor lines, such as the $5_{3,2} - 4_{4,1}$ transition at 620.701 GHz.

summit of Mauna Kea¹. The L_1/L_2 factor varies by about 15-20% across the tuning range of the SMA LOs (620-700 GHz), so it is not negligible.

The 230/690 SMA observations recorded on January 28, 2005 have been analyzed to search for correlations of phase between the two frequency bands. Figure 7 shows a time series comparison of the 215 GHz phase averaged across the central six spectral channels of the SiO maser line with the 658 GHz phase averaged across the central 21 spectral channels of the H₂O maser line. The baseline-based phase measurements were converted to antenna-based phases using the selfcal function of Miriad [13]. The gains were derived independently for each receiver band, using antenna 6 as the reference antenna, and are shown in Figure 8. The gains are plotted against each other in Figure 9 using the smavarpft function of Miriad, and the resulting linear regression results are listed in Table III. In summary, good correlations are seen on antennas 1, 2 and 3, with antenna 1 exhibiting a slope closest to the expected theoretical ratio (based on the model in Figure 6). Antenna 4 exhibited anomalous relative phases between the two frequency bands on many nights of the observing campaign, and clearly had some instrumental problem. Nevertheless, the fact that much of the phase data are well-correlated between the two bands is a promising sign for future phase referencing at the SMA. A similar analysis has been done with the lower-sideband continuum data on the minor planet Ceres (diameter 0.5'') observed for 3.5 hours on February 18, 2005 (see Figure 10). The linear regression results are also listed in Table III. Figure 11 shows a comparison of images of Ceres which demonstrates that phase transfer can be done successfully between the two receiver bands. The image in the left panel results from running selfcal on the 690 GHz data, and the signal-to-noise ratio is 267. The

¹Based on calculations performed with the *am* atmospheric model [12], available at <http://cfarx6.cfa.harvard.edu/am>

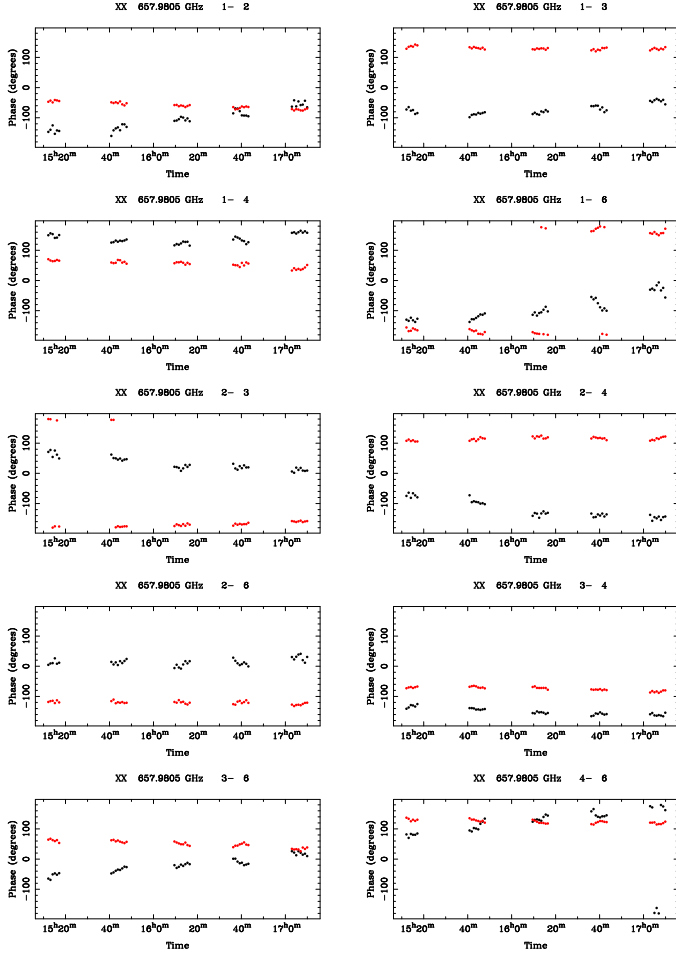


Fig. 7. Time series comparison of the spectral line maser phases of the evolved star W Hydra in the 215 GHz SiO maser (red dots) and the 658 GHz H₂O maser (black dots). The ten panels correspond to the ten different SMA baselines, as observed with five antennas on January 28, 2005.

image in the right panel results from running selfcal on the 230 GHz data, scaling the solutions to 690 GHz, and applying the scaled solutions to the 690 GHz raw data. In this case, the signal-to-noise ratio is 193.

IV. CONCLUSIONS

The SMA has successfully observed celestial sources in two frequency bands simultaneously (230 and 690 GHz). The first astronomical images with one arcsecond angular resolution in the 690 GHz band have been acquired. Initial observations of sources with strong maser lines in both bands demonstrate good correlation between the phases in the two widely-separated frequency bands, at least on most of the antennas. Although a number of instrumental issues with the SMA remain to be explored and improved, this initial result bodes well for future attempts at phase referencing the interferometer calibration from low frequencies to high frequencies in the submillimeter band (and perhaps the terahertz band), and thereby improving the ultimate sensitivity of traditional heterodyne interferometers at high frequencies.

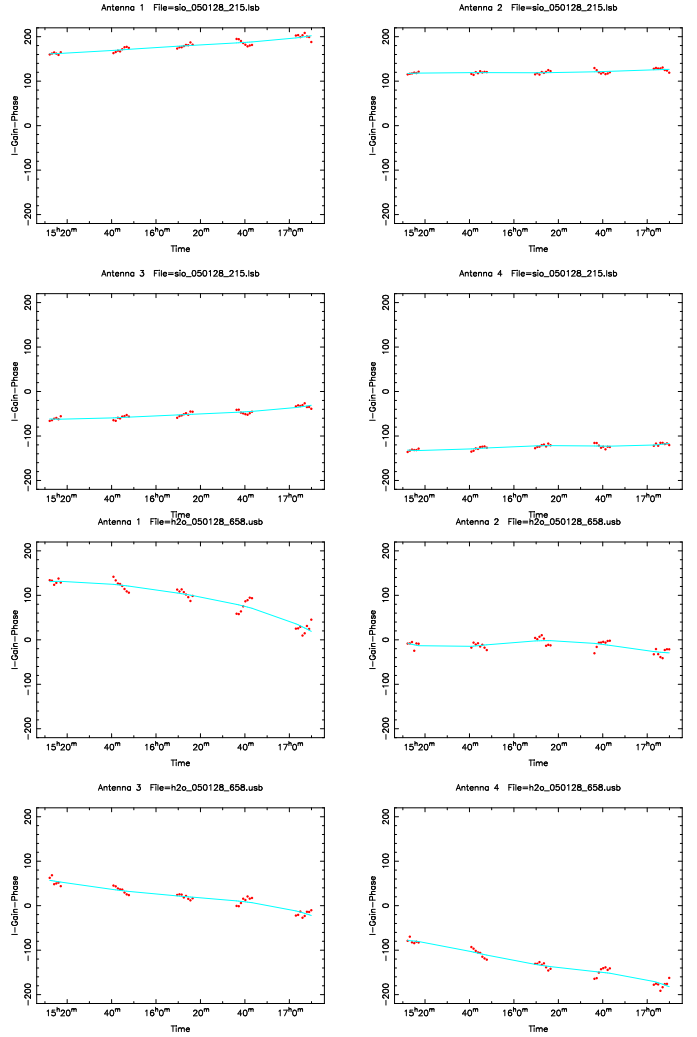


Fig. 8. Point-source antenna-based phase solutions for the SiO 215 GHz maser data (upper four panels) and the H₂O 658 GHz maser data (lower four panels) for W Hydra as observed on January 28, 2005. The reference antenna was antenna 6 whose phase was defined to be zero at all times (not shown). The phase data are plotted against each other in Figure 9.

TABLE III

LINEAR REGRESSION ANALYSIS OF THE 690 GHz BAND PHASE VS THE 230 GHz BAND PHASE OBSERVED ON W HYDRA AND CERES

Source	Antenna	Sideband	Correlation	Slope
W Hydra (28Jan2005)	1	USB	0.97	-2.77
	2		0.76	-2.04
	3		0.96	-2.17
	4		0.86	-5.03
	theory		1.00	-2.90
Ceres (18Feb2005)	1	USB	0.97	2.81
	2		0.88	2.13
	3		0.95	2.08
	4		0.90	2.22
	5		0.97	3.14
theory	1.00	3.15		
Ceres (18Feb2005)	1	LSB	0.98	3.11
	2		0.86	2.22
	3		0.92	2.19
	4		0.79	2.37
	5		0.96	3.36
theory	1.00	3.16		

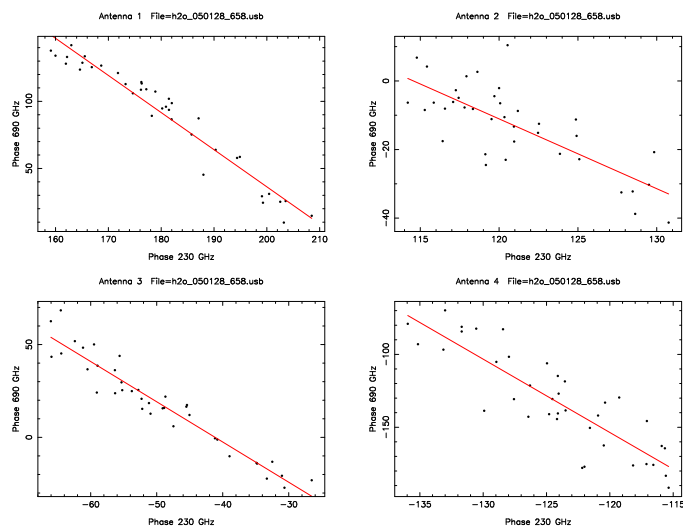


Fig. 9. Plot of the 658 GHz phase vs 215 GHz phase data from Figure 8 with linear regression fits overlaid. The negative slope results from the fact that the lower sideband SMA data are written with an opposite sign convention to the upper sideband SMA data. On antenna 1, the magnitude of the slope is close to the expected theoretical value of -2.90 , as seen in Table III.

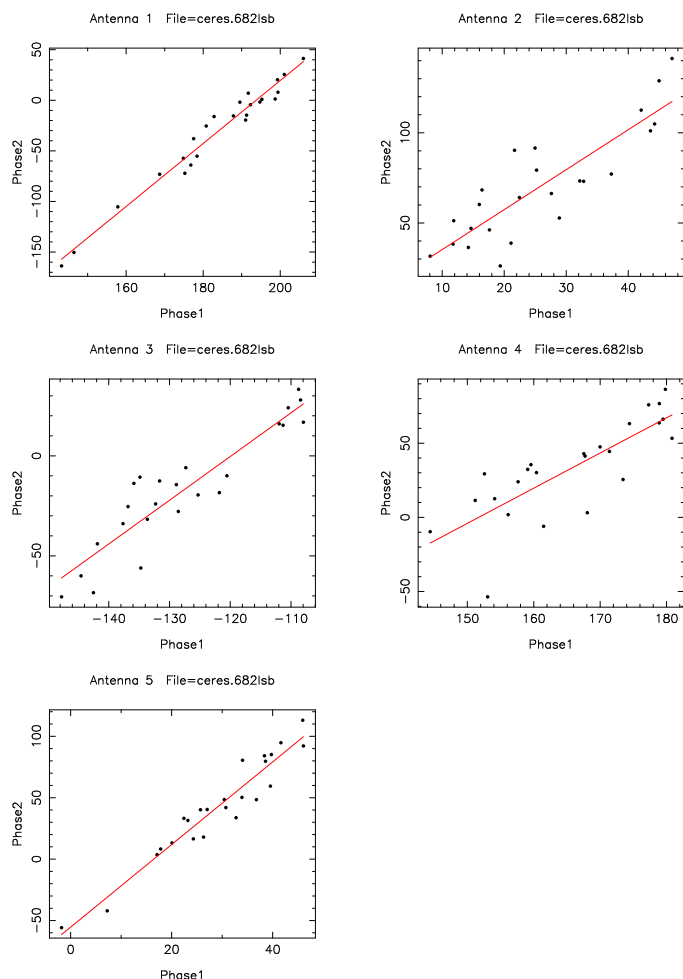


Fig. 10. Plot of the 682 GHz vs 221 GHz antenna-based continuum phase solutions of Ceres with linear regression fits overlaid. On antennas 1 and 5, the magnitude of the slope is close to the expected theoretical value of 3.15 , as seen in Table III.

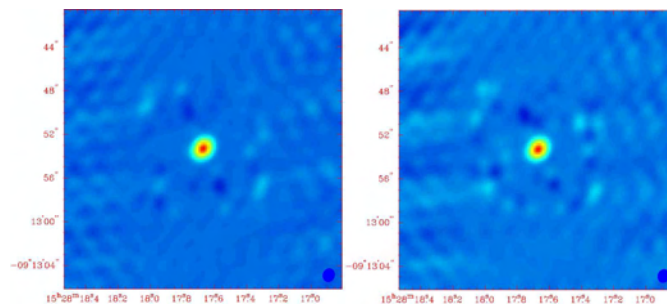


Fig. 11. Left image: the image resulting from a standard selfcal solution computed from the raw 690 GHz data of Ceres and applied to the same data. Peak = 3.53 Jy, rms= 13 mJy, SNR= 267 . Right image: the result of taking the standard selfcal solution at 230 GHz, scaling it to 690 GHz via the slope and offset (Table III), and applying it the 690 GHz raw data. Peak = 3.34 Jy, rms= 17 mJy, SNR= 193 . The degree to which the images are similar verifies the promise of this technique.

ACKNOWLEDGMENT

The authors would like to thank Irwin Shapiro for supporting the development of the SMA from its inception.

REFERENCES

- [1] R. Blundell, "The Submillimeter Array – Antennas and Receivers," in *Fifteenth International Symposium on Space Terahertz Technology*, 2004.
- [2] P. T. P. Ho, J. M. Moran, and K. Y. Lo, "The Submillimeter Array," *The Astrophysical Journal Letters*, vol. 616, p. 1, 11 2004.
- [3] K. H. Young, T. R. Hunter, D. J. Wilner, M. A. Gurwell, J. W. Barrett, R. Blundell, R. Christensen, N. Hirano, P. T. P. Ho, S. Y. Liu, K. Y. Lo, R. Martin, S. Matsushita, J. M. Moran, N. Ohashi, D. C. Papa, N. Patel, F. Patt, A. Peck, C. Qi, M. Saito, A. E. Schinckel, H. Shinnaga, T. Sridharan, S. Takakuwa, C. E. Tong, and D. Trung, "Submillimeter Array Observations of CS J = 14-13 Emission from the Evolved Star IRC+10216," *The Astrophysical Journal Letters*, vol. 616, pp. L51–L54, 11 2004.
- [4] S. T. K., M. Saito, N. A. Patel, and R. D. Christensen, "Holographic surface setting of the Sub-millimeter Array antennas," in *Proceedings of the SPIE: Ground-based Instrumentation for Astronomy*, vol. 5495, 2004, pp. 441–446.
- [5] C.-Y. Tong, D. V. Meledin, D. P. Marrone, S. N. Paine, H. Gibson, and R. Blundell, "Near-field vector beam measurements at 1 THz," *IEEE Microwave and Wireless Components Letters*, vol. 13, pp. 235–237, 2003.
- [6] T. R. Hunter, R. W. Wilson, R. Kimberk, P. S. Leiker, and R. Christensen, "Receiver control for the Submillimeter Array," in *Proceedings of the SPIE: Advanced Telescope and Instrumentation Control Software II*, vol. 4848, 12 2002, pp. 206–217.
- [7] O. P. Lay, "Phase calibration and water vapor radiometry for millimeter-wave arrays," *Astronomy and Astrophysics Supplement*, vol. 122, pp. 547–557, May 1997.
- [8] E. Middelberg, A. L. Roy, R. C. Walker, and H. Falcke, "VLBI observations of weak sources using fast frequency switching," *Astronomy and Astrophysics*, vol. 433, pp. 897–909, 4 2005.
- [9] M. A. Holdaway and L. D'Addario, "Simulation of Atmospheric Phase Correction Combined with Instrumental Phase Calibration," NRAO LAMA Memo Series, Tech. Rep. 803, 2003.
- [10] A. Thompson, J. M. Moran, and G. W. Swenson, *Interferometry and Synthesis in Radio Astronomy*. Krieger Publishing Company, 1991.
- [11] M. A. Holdaway and J. R. Pardo, "Atmospheric Dispersion and Fast Switching Phase Calibration," NRAO ALMA Memo Series, Tech. Rep. 404, 2001.
- [12] S. N. Paine, "The *am* Atmospheric Model," Submillimeter Array Project, Tech. Rep. 152, 2004, <http://sma-www.cfa.harvard.edu/private/memos/152-03.pdf>.
- [13] R. J. Sault, P. J. Teuben, and M. C. H. Wright, "A Retrospective View of MIRIAD," in *ASP Conference Series: Astronomical Data Analysis Software and Systems IV*, vol. 77, 1995, pp. 433–436.